Check for updates

Controlling electrochemical lignin depolymerization *via* halide chemistry at boron-doped diamond electrodes

Busarakham Ngokpho,[a] Pattarawadee Therdkatanyuphong,[b] Panot Krukkratoke,[b] Tanatorn Khotavivattana, [c] Apichat Boontawan[d] and Kamonwad Ngamchuea [*a]

Lignin, a highly abundant yet underutilized biopolymer, holds significant potential as a renewable source of aromatic chemicals. Herein, we present a sustainable electrochemical approach for lignin valorization, in which oxidative pathways are tunable *via* halide redox chemistry. Using boron-doped diamond electrodes, chosen for their wide potential window, high current efficiency, and fouling resistance, we elucidate the roles of halide (Cl⁻, Br⁻, I⁻) and membrane configuration in governing electrochemical reactivity, selectivity, and surface stability. Cyclic voltammetry and extended electrolysis reveal distinct regimes: chloride and bromide mediate direct electrode-driven oxidation which suffers from surface passivation, whereas iodide enables solution-phase oxidation *via* electrogenerated iodine species, minimizing fouling and delivering the highest yield of aromatic products. Product analysis confirms β-O-4 cleavage as the dominant depolymerization route, with vanillin as the primary product. Incorporation of a cation-exchange membrane substantially enhances yields and promotes deeper oxidative transformations, such as the formation of isovanillic and furan carboxylic acids. These findings define key parameters for achieving sustainable and tunable electrochemical lignin conversion without the need for sacrificial oxidants.

1 Introduction

Lignin, the second most abundant biopolymer on Earth, accounts for up to 30% of lignocellulosic biomass by weight and as much as 40% of its energy content.[1] Each year, millions of tons of lignin is generated as a by-product from the pulp and paper industry and cellulosic ethanol production, in addition to substantial amounts being present in agricultural residues such as sugarcane bagasse, maize stalks, and rubberwood. Despite its high aromatic content, lignin is overwhelmingly under-exploited, with the majority still incinerated for low-grade heat, an inefficient fate that squanders its potential as a renewable source for valuable carbon-based chemicals.[2]

Structurally, lignin is a complex, amorphous macromolecule composed of 4-hydroxyphenyl (H), guaiacyl (G), and syringyl (S) units linked by a heterogeneous array of ether (*e.g.* β-O-4) and carbon–carbon (*e.g.* β–β, β-5) bonds.[3] Among these, β-O-4 linkages are the most prevalent and represent key targets for depolymerization. Their cleavage yields high-value aromatic monomers such as vanillin, guaiacol, and 4-hydroxybenzaldehyde, relevant to the pharmaceutical, flavor, fragrance, and polymer industries.

Converting lignin into value-added chemicals, however, remains a formidable challenge. Its structural heterogeneity, extensive cross-linking, and chemical recalcitrance have historically impeded its efficient transformation.[4] Conventional approaches, including pyrolysis, enzymatic treatment, and chemical catalysis, have achieved partial success by cleaving key interunit bonds or introducing functional groups at the α- and β-positions.[5,6] However, these methods typically require harsh reaction conditions, including high temperatures and pressures, as well as stoichiometric or non-recyclable metal catalysts. These approaches are frequently constrained by catalyst deactivation, scalability issues, and environmental or economic concerns, limiting their industrial applicability.

Electrochemical depolymerization has emerged as a promising and sustainable approach for lignin valorization. By employing electrons as clean and tunable redox agents, electrooxidation facilitates bond cleavage under mild conditions. At the molecular level, anodic oxidation of lignin can activate C_α sites, cleave C–O linkages, and trigger retro-aldol reactions at C_β positions, thereby generating a diverse array of

aSchool of Chemistry, Institute of Science, Suranaree University of Technology, 111 University Avenue, Suranaree, Muang, Nakhon Ratchasima 30000, Thailand. E-mail: kamonwad@g.sut.ac.th; Tel: +66 44 224 637

bInstitute of Research and Development, Suranaree University of Technology, 111 University Avenue, Suranaree, Muang, Nakhon Ratchasima, 30000, Thailand

cCenter of Excellence in Natural Products Chemistry, Department of Chemistry, Faculty of Science, Chulalongkorn University, Bangkok, 10330, Thailand

dSchool of Biotechnology, Institute of Agricultural Technology, Suranaree University of Technology, 111 University Avenue, Suranaree, Muang, Nakhon Ratchasima 30000, Thailand

high-value products including ketones, aldehydes, carboxylic acids, and phenolic monomers.[7] Crucially, electrochemical systems allow precise modulation of redox environments *via* applied potentials or currents, enabling control over reaction pathways and product selectivity with a level of tunability that is difficult to achieve by conventional catalytic methods.

Two principal strategies have been employed for lignin electrooxidation: direct oxidation at the electrode interface and indirect oxidation mediated by solution-phase redox shuttles.[8] Direct oxidation, typically using catalytic metal or carbon-based electrodes, offers operational simplicity and direct electron transfer to lignin functional groups.[9–12] However, this approach is frequently constrained by electrode fouling, limited selectivity, and the use of hazardous or cost-prohibitive materials (*e.g.* Ni, Pb, Pt).[13] Indirect electrooxidation, on the other hand, decouples lignin oxidation from the electrode surface through the use of redox-active mediators such as polyoxometalates,[14] Fe(III) salts,[15] and nitro-aromatic species.[16] These mediators undergo reversible redox cycling at the electrode and subsequently oxidize lignin in solution, thereby mitigating surface passivation and enabling access to alternative oxidative pathways. Importantly, the continuous regeneration of mediators under mild electrochemical conditions presents a sustainable and tunable platform for lignin depolymerization.

Halide ions (Cl⁻, Br⁻, I⁻), despite being ubiquitous in electrochemical systems, have received surprisingly little attention as mediators in lignin depolymerization. Upon anodic activation, they generate reactive halogen species capable of promoting oxidative bond cleavage,[17] yet their distinct reactivities and influence on product selectivity within complex lignin matrices remain insufficiently understood. Beyond mediator identity, parameters such as electrode composition, electrolyte, and electrochemical cell design critically shape depolymerization outcomes.

In this work, we present a comprehensive electrochemical strategy to address these gaps in lignin valorization. By systematically examining the roles of electrode material, electrolyte composition, redox mediator identity, and cell architecture, we uncover key parameters that govern reactivity and product selectivity. Particular emphasis is placed on halide-mediated oxidation and the influence of membrane compartmentalization (Scheme 1), both of which are shown to critically impact depolymerization efficiency and aromatic monomer yield. Real-time kinetic analysis further reveals how electrochemical conditions shape lignin degradation pathways. These findings offer mechanistic insight and design principles to support the development of scalable, sustainable approaches for converting lignin into high-value aromatic chemicals.

2 Experimental

2.1 Chemical reagents

All reagents were of analytical grade and used as received without further purification: sodium hydroxide (NaOH, >99.0%, Sigma-Aldrich), potassium sulfate (K₂SO₄, ≥99.0%, QRëC), potassium chloride (KCl, >99.5%, Chemical Express), potassium bromide (KBr, 99.0%, Sigma-Aldrich), potassium iodide (KI, 99.0%, Sigma-Aldrich), hydrochloric acid (HCl, 37%, RCI Labscan), nitrogen gas (N₂, >99.0%, Thai Special Gas Co., Ltd.), and deionized water (18.2 MΩ cm, Elga Labwater, UK).

Alkali lignin was obtained from TCI Chemicals and is derived from needle-leaved and broad-leaved trees. According to the supplier, it was processed *via* sodium sulfite pulping, followed by partial desulfonation, oxidation, hydrolysis, and demethylation. The reported pH range is 8.0–10.0 (50 g L⁻¹, 20 °C).
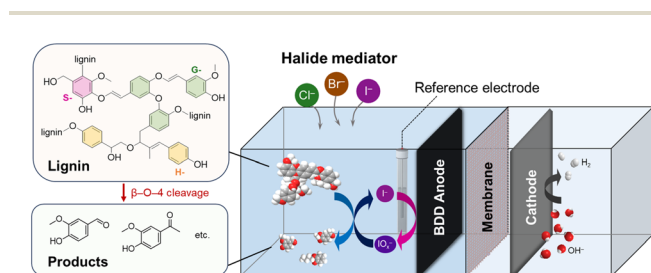
2.2 Characterization of lignin

Lignin samples were characterized by matrix-assisted laser desorption/ionization time-of-flight mass spectrometry (MALDI-TOF MS, JEOL JMS-S3000, Japan) in positive ion mode. Dihydroxybenzoic acid (DHB), dissolved in a 30 : 70 (v/v) acetonitrile/0.1% trifluoroacetic acid (TFA) mixture, was used as the matrix. The instrument was calibrated with PEG600, and the analysis was performed using a laser intensity of 67%, laser frequency of 250 Hz, and a total of 4250 laser shots. Key voltages included 20 kV for the target plate and −1625 V for the detector. The system operated under high vacuum with analyzer pressure maintained at 2.1×10^{-5} Pa.

NMR spectra were recorded on a Bruker AVANCE III 500 MHz spectrometer equipped with a CPP BBO 500S1 BB-H&F-D-05 Z probe head with *z*-gradients. Lignin samples were prepared by dissolving 60 mg of material in 0.5 mL of DMSO-d₆, and chemical shifts were referenced to the residual solvent peaks at 2.49 ppm for ¹H and 39.5 ppm for ¹³C. The spectrometer operated at 500.36 MHz for ¹H and 125.82 MHz for ¹³C, with all experiments conducted at a constant temperature of 25 °C. HSQC spectra were acquired using the Hsqcetgpprsisp2.2 pulse program, with spectral widths of 3.0 kHz (¹H) and 9.3 kHz (¹³C). A relaxation delay of 1.5 seconds was employed, and 90° pulse widths were set to 12.0 μs for ¹H and 9.5 μs for ¹³C.

2.3 Electrochemical studies

2.3.1 Cyclic voltammetry. Cyclic voltammetry studies were carried out in unstirred, N₂-saturated aqueous solutions using a PalmSens4 potentiostat (PalmSens, Netherlands) and a standard three-electrode system in a Faraday cage thermostated at 25 °C. A platinum (Pt, 2.0 mm diameter, CH Instruments, USA), gold (Au, 2.0 mm diameter, CH Instruments, USA), silver (Ag,

Scheme 1 Schematic representation of the halide-mediated electrochemical depolymerization of lignin. The left panel illustrates the representative lignin structure comprising typical monolignol units (G, H, and S) and aromatic products formed *via* β-O-4 bond cleavage.

2.0 mm diameter, CH Instruments, USA), glassy carbon (GC, 3.0 mm diameter, ItalSens, Netherlands), graphite (6.0 mm diameter, X2 Lab, China), or boron-doped diamond (BDD, 3.0 mm diameter, Windsor Scientific, UK) was used as a working electrode. Prior to use, the working electrode was polished with water–alumina slurry (1.0, 0.3, and 0.05 μm, Buehler, USA) on soft lapping pads (Buehler, USA). A silver/silver chloride electrode (Ag/AgCl in saturated KCl, ItalSens, Netherlands) and a platinum sheet were used as reference and counter electrodes, respectively.

2.3.2 Extended electrolysis. Electrolysis of lignin was carried out in both undivided and divided electrochemical cells under potentiostatic control to investigate the influence of halide mediators and membrane configurations. A custom-made, double-walled glass H-cell was employed for the divided setup, with cation-exchange membrane (CEM, Fumaseps FKS-PET-130, Fumatech, Germany) or anion-exchange membrane (AEM, Fumaseps FAA-3-PK-130, Fumatech, Germany) used to compartmentalize the catholyte and anolyte. Each compartment contained 35 mL of electrolyte: the anolyte comprised lignin in 1.0 M NaOH with a selected halide (KCl, KBr, or KI), while the catholyte contained blank 1.0 M NaOH electrolyte. All electrolysis experiments were conducted using a three-electrode configuration, consisting of a BDD working electrode, a platinum counter electrode, and a Ag/AgCl (saturated KCl) reference electrode. The uncompensated solution resistance (R_s) was determined by electrochemical impedance spectroscopy (EIS, frequency $1–10^5$ Hz, amplitude 5 mV) to be 4.2 Ω. At the maximum current of 15 mA, the resulting iR drop was 0.063 V. The electrolyte pH was maintained at 14. A constant potential of 1.4 V $vs.$ Ag/AgCl (equivalent to 2.36 V $vs.$ RHE after correction for solution resistance) was applied for up to 4 hours using a PalmSens4 potentiostat (PalmSens, Netherlands). Aliquots were collected at designated intervals for subsequent UV-vis kinetic analysis (Section 2.4) and GC-MS product characterization (Section 2.5).

2.4 Monitoring of lignin depolymerization kinetics

Lignin degradation kinetics in the presence of halide ions (Cl^-, Br^-, or I^-) was monitored using UV-vis spectroscopy (UV-1900i, Shimadzu, Japan). Absorbance spectra were recorded between 220 and 600 nm at 30 minute intervals over a total duration of 240 minutes.

2.5 Characterization of lignin depolymerization products

Following electrolysis, the anolyte was acidified to pH 2 using hydrochloric acid and subjected to liquid–liquid extraction with ethyl acetate in a 1 : 1 volume ratio.[18,19] The organic layer was collected, dried over anhydrous sodium sulfate, and filtered. The resulting extract was analyzed by gas chromatography-mass spectrometry (GC-MS, Agilent Technologies 7000, USA). To improve the volatility and detectability of phenolic compounds, the samples were derivatized with N,O-bis(trimethylsilyl)trifluoroacetamide (BSTFA) prior to injection. Separation was performed using an HP-5MS capillary column (60 m length, 0.25 mm inner diameter, 2 μm DB-WAX stationary phase) with

helium as the carrier gas at a flow rate of 5 mL min^{-1}. The oven temperature program was as follows: initial hold at 150 °C for 5 min, ramp at 15 °C min^{-1} to 250 °C, and hold for 20 min. The injector temperature was maintained at 280 °C, and mass spectrometric detection was conducted in electron impact (EI) mode with an ionization voltage of 70 eV. For quantitative analysis, 1,4-dihydroxybenzene was used as an internal standard.[20,21]

3 Results and discussion

Herein, we investigate lignin electro-depolymerization through integrated structural, electrochemical, and molecular-level analyses. Initial characterization revealed key subunits and linkages within the lignin sample. Electrochemical studies evaluated redox behavior across different electrode materials. The role of halide-derived redox mediators was comprehensively examined under both dynamic and sustained electrolysis conditions. Temporal monitoring of lignin degradation provided insight into reaction kinetics, while downstream analysis of products elucidated oxidation pathways and selectivity. The influence of membrane configuration on product distribution and transformation efficiency was also assessed.

3.1 Structural features of lignin

The structural features of lignin were elucidated using MALDI-TOF mass spectrometry and 2D NMR (HSQC) spectroscopy. The combined data reveal that the lignin sample was composed predominantly of guaiacyl (G) and 4-hydroxyphenyl (H) units, with no evidence of syringyl (S) units.

The MALDI-TOF MS spectrum (Fig. 1a) displays a series of peaks in the range of m/z 191–473. The low-mass peaks at m/z 191 and 221 are assigned to G-type and H-type monomers, respectively, while higher-mass peaks correspond to dimers and trimers with β-O-4 and β–β linkages. Representative structures matching these masses are shown in Fig. 2. It should be emphasized, however, that each m/z peak may correspond to multiple isomeric structures, and the proposed structures serve as plausible, literature-supported assignments rather than definitive identifications.[22,23] Additionally, signals above m/z 500 were not observed, which is commonly reported in MALDI-TOF MS analysis of lignin.[24] This is primarily attributed to the lower ionization efficiency of high-molecular-weight oligomers and the tendency of labile ether linkages to undergo fragmentation during laser desorption/ionization. Nevertheless, the observed low-mass region provides valuable structural information, capturing the dominant monomeric and oligomeric units and enabling the identification of key interunit linkages such as β-O-4 and β–β. These observations highlight the dominant interunit linkages and provide structural insight relevant to lignin's reactivity and valorization.

The HSQC spectrum provides detailed correlations between ^1H and ^{13}C nuclei, enabling identification and semi-quantitative analysis of lignin substructures. In the aromatic region (Fig. 1b), signals at δ_C/δ_H of 112/6.9 ppm, 115/6.8 ppm, and 121/6.7 ppm correspond to G_2, G_5/G_6, and G_5/G_6,[25–27] arising
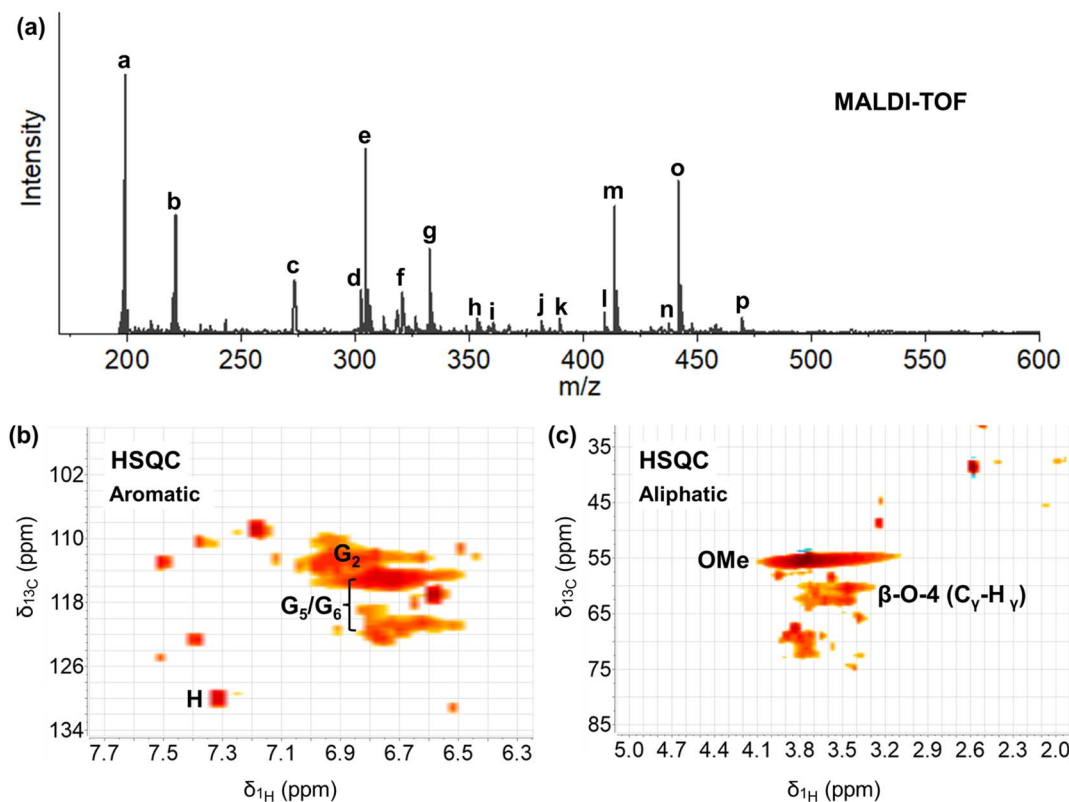
Fig. 1 (a) MALDI-TOF MS spectrum of lignin in positive ion mode. (b) and (c) HSQC spectra of lignin in the aromatic and aliphatic regions, respectively.

from protons at C_2, C_5, and C_6 positions on the guaiacyl (G) ring. An additional signal was observed at 130/7.3 ppm, characteristic of the 4-hydroxyphenyl (H) unit. Integration of cross-peak volumes reveals a G : H ratio of approximately 7 : 1, indicating the guaiacyl-rich nature of the lignin sample. No cross-peaks indicative of S units were observed.

In the aliphatic region (Fig. 1c), cross-peaks at ∼60/3.4 ppm correspond to C_γ–H_γ in etherified structures, while signals associated with β–β linkages (∼53–54/3.0–3.2 ppm) appear only as minor components.[25,26,28,29] These observations confirm that β-O-4 is the predominant interunit linkage in the lignin polymer.

3.2 Cyclic voltammetry of lignin electrooxidation

3.2.1 Effect of electrode material on transient voltammetric behavior. The electrochemical behavior of lignin was first evaluated using cyclic voltammetry (CV) across a series of metallic and carbonaceous macroelectrodes, platinum (Pt), gold (Au), silver (Ag), glassy carbon (GC), graphite, and boron-doped diamond (BDD), to identify a suitable platform for oxidative depolymerization (Fig. 3). These electrodes were selected to provide a comprehensive comparison of surfaces with diverse electrochemical properties. Noble metals (Pt, Au, and Ag) are well known for their fast electron transfer kinetics and high conductivity, while carbon-based electrodes (GC, graphite, and BDD) offer wide potential windows, distinct

surface chemistry, and enhanced resistance to surface fouling.[30–32]

The CVs of lignin at all electrodes revealed irreversible oxidation behavior, as evidenced by the absence of reduction peaks in the reverse scans, consistent with the multistep, non-reversible oxidation of phenolic and ether-containing structures in lignin.[33] On noble metal electrodes, Pt (Fig. 3a) and Au (Fig. 3b) exhibited single oxidation peaks at $E_p = 0.37$ V ($i_p = 0.78$ A m^{-2}) and $E_p = 0.70$ V ($i_p = 1.54$ A m^{-2}), respectively. Similarly, carbon-based electrodes, GC (Fig. 3d) and graphite (Fig. 3e), showed irreversible oxidation peaks at $E_p = 0.69$ V ($i_p = 4.67$ A m^{-2}) and $E_p = 0.58$ V ($i_p = 5.54$ A m^{-2}), respectively. In contrast, no oxidative signal attributable to lignin was observed on the Ag electrode (Fig. 3c) due to competing surface reactivity and parasitic reactions involving silver itself which suppress or obscure the electrochemical response associated with lignin oxidation.

Among all the electrodes tested, BDD (Fig. 3f) demonstrated the most distinct and promising behavior. Two well-defined anodic peaks were observed at $E_{p,1} = 0.36$ V and $E_{p,2} = 0.80$ V, with current densities of 1.68 and 3.10 A m^{-2}, respectively. The appearance of two anodic features is consistent with sequential oxidation steps of lignin. While we refrain from assigning a unique, electrode-specific mechanism on the basis of CV alone, the sharper peak definition and broad accessible potential window on BDD motivate its selection for detailed investigation in the remainder of the study.
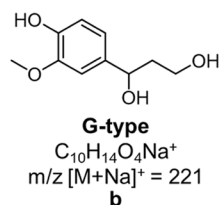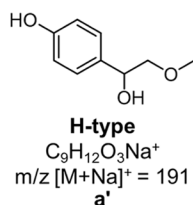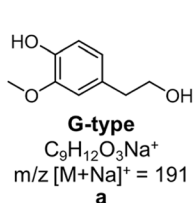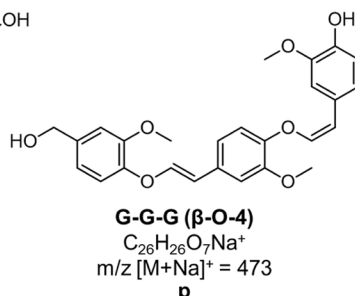
Monomers

G-type
$C_9H_{12}O_3Na^+$
m/z $[M+Na]^+$ = 191
a

H-type
$C_9H_{12}O_3Na^+$
m/z $[M+Na]^+$ = 191
a'

G-type
$C_{10}H_{14}O_4Na^+$
m/z $[M+Na]^+$ = 221
b

β-O-4 linkages

G-H (β-O-4)
$C_{16}H_{16}O_3Na^+$
m/z $[M+Na]^+$ = 279
c

G-H (β-O-4)
$C_{18}H_{18}O_3Na^+$
m/z $[M+Na]^+$ = 305
d

G-H (β-O-4)
$C_{18}H_{20}O_3Na^+$
m/z $[M+Na]^+$ = 307
e

G-G (β-O-4)
$C_{19}H_{20}O_4Na^+$
m/z $[M+Na]^+$ = 335
g

G-G (β-O-4)
$C_{19}H_{22}O_5Na^+$
m/z $[M+Na]^+$ = 353
h

G-G (β-O-4)
$C_{18}H_{22}O_6Na^+$
m/z $[M+Na]^+$ = 357
i

G-G (β-O-4)
$C_{19}H_{24}O_7Na^+$
m/z $[M+Na]^+$ = 387
k

G-G (β-O-4)
$C_{20}H_{26}O_7Na^+$
m/z $[M+Na]^+$ = 401
l

G-G (β-O-4)
$C_{20}H_{26}O_8Na^+$
m/z $[M+Na]^+$ = 417
m

G-G (β-O-4)
$C_{21}H_{28}O_8Na^+$
m/z $[M+Na]^+$ = 431
n

G-G-G (β-O-4)
$C_{26}H_{26}O_7Na^+$
m/z $[M+Na]^+$ = 473
p

β-β linkages

G-G (β-β)
$C_{18}H_{18}O_4Na^+$
m/z $[M+Na]^+$ = 321
f

G-G (β-β)
$C_{20}H_{22}O_6Na^+$
m/z $[M+Na]^+$ = 381
j

G-G (β-β)
$C_{24}H_{30}O_6Na^+$
m/z $[M+Na]^+$ = 437
o
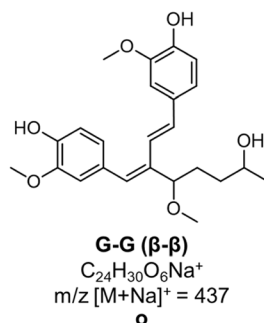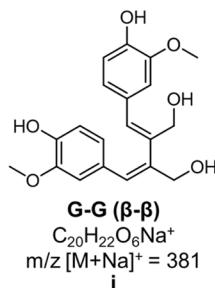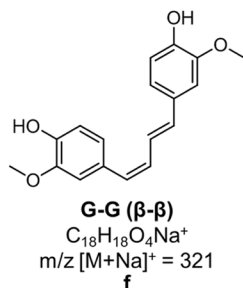
Fig. 2 Representative structural components and interunit linkages of lignin. Structures (a–p) correspond to MALDI-TOF MS peaks in Fig. 1a and are grouped by linkage type (not alphabetical order).

3.2.2 Effect of halide identity and concentration. To investigate the role of halide mediators in lignin electro-oxidation, cyclic voltammetry of lignin was performed at a BDD electrode in the presence of varying concentrations (0–100 mM) of KCl, KBr, or KI. In chloride- (Fig. 4a) and bromide-containing systems (Fig. 4b), a modest enhancement in oxidative peak
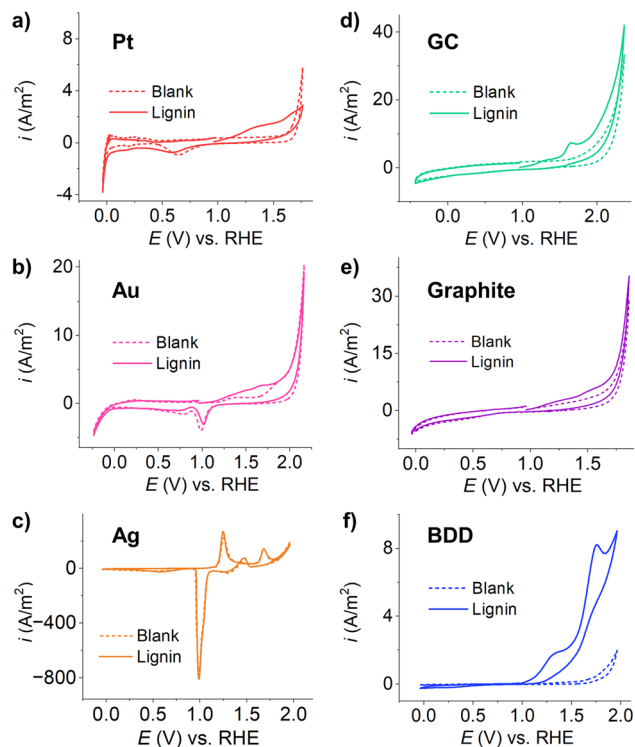
Fig. 3 Cyclic voltammograms (10 mV s^{-1}, 25 °C) of 2.0 g per L lignin in 1.0 M NaOH with 18 mM KCl at (a) Pt, (b) Au, (c) Ag, (d) GC, (e) graphite, and (f) BDD electrodes.

BrO$_x$$^{-}$), are not produced in sufficient concentrations at these potentials to induce homogeneous lignin oxidation in the solution phase. The observed increase in peak current is attributed to interfacial effects from trace halogen species that transiently alter the electrode/electrolyte interface such as double-layer properties and the extent of electrode fouling.[34,35]

In contrast, iodide-containing systems (Fig. 4c) exhibited markedly different behavior. Increasing I^{-} concentration led to a significant suppression of the net oxidation current of lignin. As shown in Fig. 4d, increasing I^{-} concentration significantly suppressed the net oxidation current of lignin, with the net peak current density ($i_{p,lignin} - i_{p,blank}$) decreasing progressively. This trend suggests that electrogenerated iodine species, such as IO$_3$$^{-}$,[36] engage in chemical reactions with lignin in solution, thereby depleting the local lignin concentration near the electrode. These chemical pathways reduce the flux of electroactive lignin to the electrode surface, leading to diminished current responses.

These findings therefore highlight distinct roles for halides in lignin electrooxidation: Cl^{-} and Br^{-} exhibit mild interfacial effects that modestly enhance electron transfer, while I^{-} acts as a chemically reactive mediator that consumes lignin prior to its electrochemical oxidation. These contrasting behaviors underscore the importance of mediator identity and concentration in tailoring oxidative pathways and current efficiency during lignin valorization. The implications of these behaviors are further explored under prolonged electrolysis conditions in Section 3.4.

3.2.3 Effect of lignin concentration. To evaluate the influence of lignin concentration on electrooxidation behavior, cyclic voltammetry was conducted at varying lignin concentrations (0–20 g L^{-1}) in the presence of KCl, KBr, or KI (Fig. 5a–c). Across all halide systems, an increase in lignin concentration leads to a progressive rise in oxidative current density,
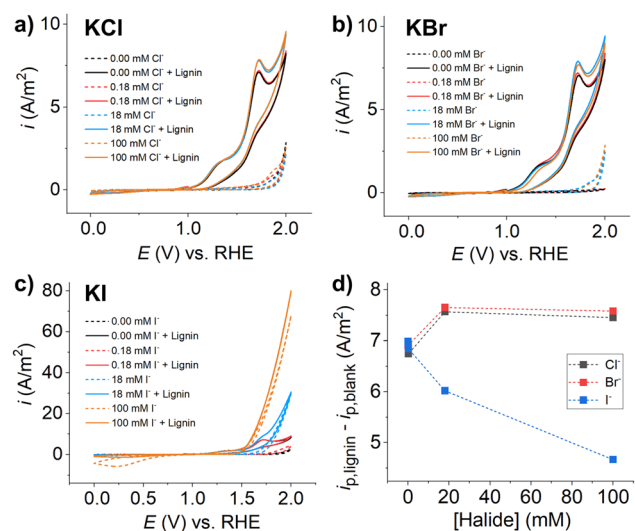
current of lignin is observed, with the effect reaching saturation at 18 mM. The peak positions and voltammetric profiles remain unchanged, and the halide-only systems exhibit no significant faradaic activity in this region. These results suggest that Cl$_2$ and Br$_2$, or their corresponding oxyhalide species (e.g. ClO$_x$$^{-}$,

Fig. 4 Cyclic voltammograms of 2.0 g per L lignin in 1.0 M NaOH (BDD electrode, 10 mV s^{-1}, 25 °C) with varying concentrations of (a) KCl, (b) KBr, and (c) KI. (d) Plot of the net oxidative peak current density ($i_{p,lignin} - i_{p,blank}$) as a function of halide concentration.
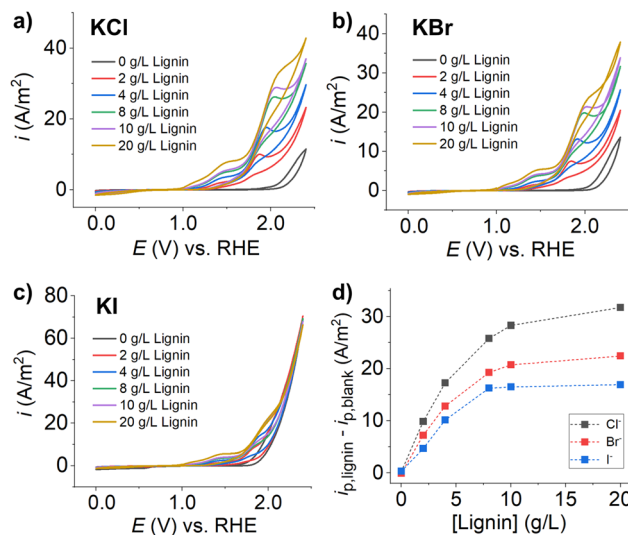

Fig. 5 Cyclic voltammograms (BDD electrode, 10 mV s^{-1}, 25 °C) of varied lignin concentrations in 1.0 M NaOH containing 18 mM of (a) KCl, (b) KBr, and (c) KI. (d) Plot of the net oxidative peak current density ($i_{p,lignin} - i_{p,blank}$) as a function of lignin concentration.

consistent with enhanced availability of redox-active phenolic units. However, the trend deviates from linearity at higher concentrations, as shown in Fig. 5d.

The sublinear response suggests that factors beyond bulk lignin availability begin to influence the observed current at elevated concentrations. Most notably, partial electrode fouling likely plays a significant role. Lignin and its oxidation products, particularly quinones and aromatic oligomers, are known to adsorb onto electrode surfaces and form passivating layers.[37] At higher lignin loadings, the accumulation of these species on the BDD surface may progressively reduce the number of available electroactive sites, thereby limiting the current response despite increasing lignin concentration in solution. In addition, at high concentrations, increased solution viscosity or potential lignin aggregation may hinder mass transport within the diffusion layer and reduce effective access to the electrode surface. Careful control of lignin loading is therefore essential for optimizing current response and minimizing electrode fouling in electrochemical valorization processes.

3.2.4   Multiple voltammetric cycling. To evaluate the effect of halide mediators on electrode surface stability, successive cyclic voltammograms of lignin were recorded at a BDD electrode in the presence of KCl, KBr, or KI (Fig. 6a–c). The progressive change in oxidative peak current over three consecutive cycles is shown in Fig. 6d.

In the Cl⁻-containing system, a notable decrease in peak current was observed with each successive cycle, indicating progressive surface passivation which results from the accumulation of lignin-derived residues or polymeric oxidation products that adhere to the electrode and impede electron transfer. Br⁻ exhibited improved current retention relative to Cl⁻, suggesting an enhanced ability to preserve electrode activity, although signs of surface deactivation remained evident in both cases.

In contrast, the I⁻ systems exhibited substantially greater retention of current across successive cycles (<4% signal loss by the third cycle), indicating superior surface stability. This minimal decline suggests that iodide effectively mitigates electrode fouling. The *in situ* generation of reactive iodine species may facilitate the oxidative degradation of adsorbed lignin residues, preventing their accumulation on the electrode. Moreover, the strong solution-phase reactivity of these species likely shifts lignin oxidation away from the electrode interface, reducing the formation of passivating surface films, consistent with the results discussed in the previous sections. These observations highlight the advantageous role of iodide in preserving electrochemical activity during repeated voltammetric cycling, a key consideration for sustained lignin valorization. The implications for long-term electrode performance under controlled-potential electrolysis are further discussed in Section 3.4.

3.2.5   Effect of scan rate. To probe the dynamic characteristics of lignin oxidation in the presence of halide redox mediators, cyclic voltammetry was performed at BDD electrodes over a range of scan rates (10–200 mV s⁻¹) in the presence of KCl, KBr, or KI (Fig. 7a–c). In all cases, increasing scan rate resulted in a progressive increase in the oxidation peak currents. Log–log plots of the net oxidative peak current density ($i_{p,lignin} - i_{p,blank}$) *versus* scan rate yielded slopes of ~0.5 (Fig. 7d), indicating mass transport (diffusion)-controlled behavior. Accordingly, enhancing convective transport, such as through stirring or flow-cell operation, could improve lignin electrooxidation efficiency, as later implemented in the extended electrolysis experiments.

3.2.6   Tafel analysis. To gain further insight into the electron transfer kinetics of lignin oxidation in halide-containing systems, mass-transport corrected Tafel analysis (eqn (1))[38] was applied to the first anodic peak observed in the cyclic voltammograms.
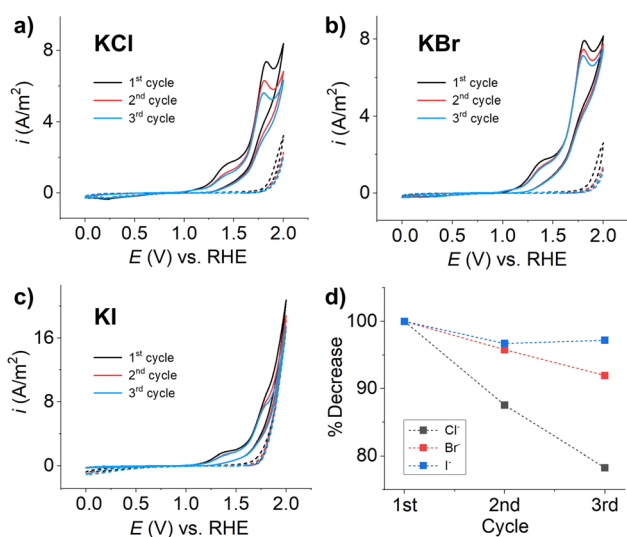

Fig. 6 Successive cyclic voltammograms (BDD electrode, 10 mV s⁻¹, 25 °C) of 2.0 g per L lignin in 1.0 M NaOH containing 18 mM of (a) KCl, (b) KBr, and (c) KI. (d) Plot of percentage decrease in oxidative peak current from the first to subsequent cycles.
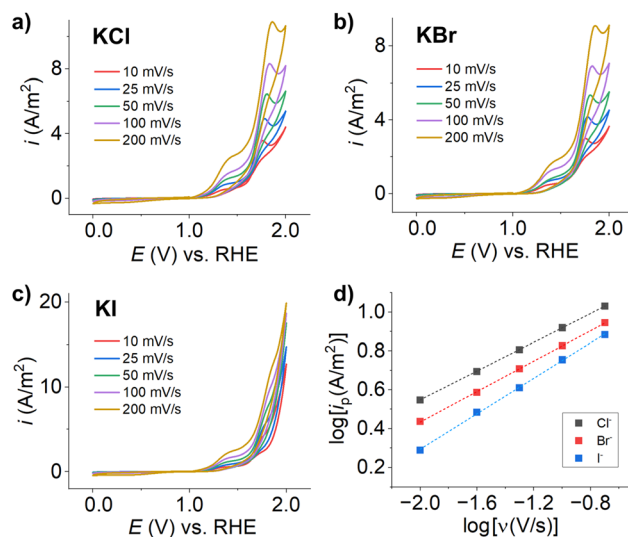

Fig. 7 Cyclic voltammograms (BDD electrode, 25 °C) of 2.0 g per L lignin in 1.0 M NaOH containing 18.0 mM of (a) KCl, (b) KBr, and (c) KI at varied scan rates (10–200 mV s⁻¹). (d) Log–log plots of the net oxidative peak current density ($i_{p,lignin} - i_{p,blank}$) *versus* scan rate.

$$\frac{\partial \ln\left(\frac{I^2 I_p}{I_p - I}\right)}{\partial E} = \frac{2F\left(n' + \beta_{n'+1}\right)}{RT}, \tag{1}$$

where the I is the current within the 10–48% range of the peak current (I_p), a region where the faradaic current dominates while capacitive and mass transport contributions are minimal. E is the electrode potential, F is the Faraday constant (96 485 C mol^{-1}), n' is the number of electron transfer before the rate determining step (RDS), $\beta_{n'+1}$ is the anodic transfer coefficient of the RDS, R is the molar gas constant (8.314 J K^{-1} mol^{-1}), and T is the absolute temperature.

The extracted $n' + \beta_{n'+1}$ values for the first oxidation peak were 0.293 ± 0.001 in Cl$^-$, 0.287 ± 0.001 in Br$^-$, and 0.284 ± 0.001 in I$^-$, indicating that the first electron transfer step is rate-determining ($n' = 0$), and thus these values correspond directly to the transfer coefficient of the RDS.

3.3 Kinetics of electrochemical lignin degradation

To complement the electrochemical analysis, the kinetics of lignin degradation were evaluated by time-resolved UV-vis spectroscopy under controlled-potential electrolysis (BDD electrode, 2.36 V *vs.* RHE, 25 °C) in the presence of KCl, KBr, or KI. The lignin solution exhibited two prominent absorption bands at 290 nm and 345 nm (Fig. 8), corresponding to π–π* transitions of conjugated aromatic systems and phenolic subunits.[39,40] A progressive decline in absorbance at both wavelengths was observed with increasing electrolysis time, consistent with cleavage of the aromatic structures in lignin.

Kinetic analysis of the absorbance decay revealed that the degradation followed a pseudo-first-order kinetics. The data fit well to the following expression:[41]

$$\ln(A/A_0) = -kt \tag{2}$$

where A is the absorbance at time t, A_0 is the initial absorbance, and k is the apparent first-order rate constant. The derived rate constants (at 345 nm) were $-(1.05 \pm 0.10) \times 10^{-3}$ min^{-1} for Cl$^-$, $-(1.00 \pm 0.06) \times 10^{-3}$ min^{-1} for Br$^-$, and $-(1.09 \pm 0.09) \times 10^{-3}$ min^{-1} for I$^-$. These values suggest that the lignin degradation rates are comparable across halide systems under the applied electrolysis conditions.

However, it is important to note that lignin degradation products, particularly oxidized phenolics and aromatic acids, may also exhibit significant absorbance in the same UV region as native lignin. This spectral overlap complicates interpretation of absorbance decay, especially at 280–350 nm, where many lignin-derived compounds also absorb.[42] Several prior studies have applied pseudo-first-order kinetic models based on UV-vis absorbance decay to quantify lignin degradation rates, often assuming that the observed signal exclusively corresponds to unreacted lignin.[40,43] Such assumptions may lead to over-estimation of degradation efficiency and underestimation of product complexity. Caution is thus warranted in using UV-vis data alone to draw mechanistic conclusions. Nonetheless, the comparable degradation rates across halide systems suggest that, under prolonged electrolysis, differences in voltammetric behavior (Section 3.2) have limited impact on the kinetics of lignin oxidative breakdown in bulk solution. These findings are revisited in Section 3.4 through analysis of product composition and electrolysis efficiency.

3.4 Extended electrolysis of lignin

To elucidate the pathways and products of lignin electro-depolymerization, controlled-potential electrolysis of lignin was performed in the presence of KCl, KBr, or KI (BDD electrodes, 2.36 V *vs.* RHE, 25 °C). The electrolysis products were analyzed by gas chromatography-mass spectrometry (GC-MS), as detailed in the Experimental section.

A range of lignin-derived aromatic products were identified, including aldehydes (*e.g.* vanillin, benzaldehyde), ketones (apocynin), carboxylic acids (isovanillic acid, 2-furancarboxylic acid, benzoic acid, homovanillic acid), and rearranged phenolic species (2-propoxyphenol, 2-methoxyphenol), as summarized in Table 1. Vanillin was the predominant product under all tested conditions, consistent with its formation from guaiacyl (G) units, the principal monomeric component of lignin as characterized in Section 3.1, *via* oxidative cleavage of β-O-4 linkages (Scheme 2).

Other products, such as isovanillic acid and homovanillic acid, also derive primarily from G units and suggest further side-chain oxidation or rearrangement of aldehydic intermediates. Notably, deeper oxidation products, particularly carboxylic acids and furan-type compounds, were observed predominantly under conditions involving both halide mediators and membrane confinement. This behavior is indicative of more aggressive oxidation regimes or localized accumulation of highly reactive species, such as hypohalites, facilitated by halide presence and membrane-induced spatial confinement.

Fig. 8 Time-resolved UV-vis absorbance spectra of 2.0 g per L lignin during electrolysis (BDD electrode, 2.36 V *vs.* RHE, 25 °C) in 1.0 M NaOH containing 18.0 mM of (a) KCl, (b) KBr, or (c) KI. (d) First-order kinetic plots of ln(A/A_0) *versus* time, where A is the absorbance at 345 nm at each time point and A_0 is the initial absorbance.

Table 1 Aromatic compounds obtained from the electrochemical depolymerization of 20 g per L alkaline lignin at a BDD electrode with a cation-exchange membrane, in the presence of 18 mM KCl, KBr, KI, or K_2SO_4 at pH 14, applied potential of 2.36 V vs. RHE for 4 hours at 25 °C

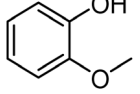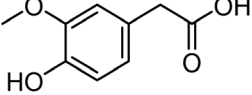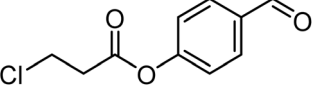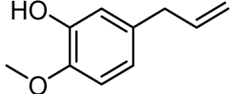| Compound	Structure	Without membrane				Anion exchange membrane				Cation exchange membrane			
		Yield (g kg^{-1} of lignin)				Yield (g kg^{-1} of lignin)				Yield (g kg^{-1} of lignin)			
		K_2SO_4	KCl	KBr	KI	K_2SO_4	KCl	KBr	KI	K_2SO_4	KCl	KBr	KI
Vanillin (4-hydroxy-3-methoxybenzaldehyde)		4.5	3.3	3.8	3.8	5.3	4.0	5.5	3.6	4.0	14.0	10.9	13.5
Apocynin (4-hydroxy-3-methoxyacetophenone)		0.5	0.5	0.5	0.7		0.4	0.7	0.5	0.9	1.2	1.1	1.8
2-Propoxyphenol						9.4							1.2
Isovanillic acid (3-hydroxy-4-methoxybenzoic acid)												1.1	0.9
2-Furancarboxylic acid									0.1	0.3	0.8	1.1	0.9
Benzaldehyde (benzenecarbaldehyde)		0.2	0.2	0.2	0.3	0.3	0.2	0.2	0.3			0.3	0.3
Benzoic acid (benzenecarboxylic acid)						12.4	0.1			0.2	0.2		
2-Methoxyphenol		0.3	0.4	0.3	0.3			0.3					
Homovanillic acid (2-(4-hydroxy-3-methoxyphenyl)acetic acid)		0.3	0.3		0.2			0.2					
(4-Formylphenyl) 3-chloropropanoate		0.4						0.4					
3-Allyl-6-methoxyphenol								0.3					

Low-molecular-weight compounds such as benzaldehyde likely result from cleavage of more condensed lignin linkages, such as β–β, which yield smaller aromatic aldehydes upon fragmentation. The appearance of 2-propoxyphenol, a non-canonical product, may be attributed to alkylation or solvolytic side reactions occurring under electrochemical conditions.

Scheme 2 Proposed mechanism for the conversion of the guaiacol (G) unit to vanillin (4-hydroxy-3-methoxybenzaldehyde), adapted from the reported mechanism for the model compound 1-(4-hydroxy-3-methoxyphenyl)-2-(2-methoxyphenoxy)-1,3-propanediol.[44]

Collectively, these structure–product relationships support a mechanistic pathway in which lignin depolymerization proceeds primarily *via* cleavage of β-O-4 linkages, followed by stepwise side-chain oxidation (alcohol → aldehyde → acid) and, in some cases, ring oxidation or fragmentation. The relative abundance of each product class was strongly influenced by the electrochemical environment, particularly halide identity and membrane configuration, as discussed in the following section.

Compared to recent electrochemical lignin valorization reports (summarized in Table 2), our system (particularly the iodide/cation-exchange membrane configuration) demonstrates strong performance in both product yield and operational simplicity. Under mild conditions (room temperature and atmospheric pressure with 1.0 M NaOH and 18 mM KI), we achieved a vanillin yield of 13.5 g kg^{-1} within 4 hours. This is comparable to or exceeds the performance of other systems operating at room temperature, such as Ni–Co/Pt ($\approx$1.3 g kg^{-1}

over 4 h)[45] and NiOOH ($\approx$1.2 g per kg vanillin, total aromatics $\approx$ 12.3 g kg^{-1}).[46] While higher vanillin yields have been reported using Pb-based anodes at elevated temperatures, these approaches often rely on toxic materials, high temperatures, or extended reaction times. In contrast, our system employs a safer anode material, operates under ambient conditions, and achieves selective production of valuable aromatics (*e.g.* vanillin, apocynin) without requiring multi-step processing or elevated temperatures.

3.4.1 Effect of membrane configuration. To assess the effect of spatial confinement on oxidant distribution and reactivity, electrolysis was performed using three different cell configurations: membrane-free, anion-exchange membrane (AEM), and cation-exchange membrane (CEM). The resulting product yields and distributions are summarized in Table 1. Both the membrane-free and AEM setups yielded relatively low amounts of lignin-derived products. In contrast, the use of

Table 2 Comparison of electrochemical lignin valorization conditions and resulting products

Anode	Electrolyte	Lignin type	Temperature/ time	Products	Ref.
PbO$_2$/NiMoCo	1 M NaOH	Corn stover lignin	40 °C/1.5 h	*trans*-Ferulic acid (22.40 g kg^{-1}), vanillin (11.09 g kg^{-1}), 3-hydroxy-4-methoxyphenyl-ethanone (2.37 g kg^{-1}), syringaldehyde (10.04 g kg^{-1}), acetosyringone (6.95 g kg^{-1}), 4-methoxy-3-methylphenol (38.83 g kg^{-1})	13
Pb/PbO$_2$	1 M NaOH	Bamboo lignin	40 °C/2 h	Vanillin (36.06 g kg^{-1}), syringaldehyde (57.30 g kg^{-1}), and *p*-coumaric acid (29.64 g kg^{-1})	47
Pb/PbO$_2$	1 M NaOH	Cornstalk lignin	30 °C/4 h	Toluene (36.1 g kg^{-1}), *m*-xylene (10.3 g kg^{-1}), *o*-xylene (12.1 g kg^{-1}), anisole (9.5 g kg^{-1})	48
Ti/SnO$_2$–Sb$_2$O$_3$/α-PbO$_2$/β-PbO$_2$	1 M NaOH	Rice straw lignin	35–55 °C/5 h	Aromatic ketones (4.09 g kg^{-1}), aromatic aldehydes (1.53 g kg^{-1}), aromatic acids (23.92 g kg^{-1})	49
Ni–Co/Pt	1 M NaOH	Alkali lignin	RT/16 h	Vanillin (0.316 g kg^{-1} h^{-1}), 3-methylbenzaldehyde (0.152 g kg^{-1} h^{-1})	45
NiOOH	1 M NaOH	Soda lignin	RT/4 h	Sinapic acid (0.32 wt%), acetovanillone (0.15 wt%), vanillin (0.12 wt%), vanillic acid (0.12 wt%) with the total aromatics of ~1.23 wt%	46
BDD	1 M NaOH/ 18 mM KI	Alkali lignin	RT/4 h	Vanillin (13.5 g kg^{-1}), apocynin (1.8 g kg^{-1}), 2-propoxyphenol (1.2 g kg^{-1}), isovanillic acid (0.9 g kg^{-1}), 2-furancarboxylic acid (0.9 g kg^{-1}), benzaldehyde (0.3 g kg^{-1})	This work

a CEM led to a substantial increase in product yield, particularly in halide-containing systems.

To quantitatively evaluate the relative contributions of competing electrochemical processes, including oxygen evolution reaction (OER), halide oxidation, and direct lignin oxidation, the charge distribution was quantified using the following definitions:

$$Q_{lignin} = Q_{total} - Q_{blank} \qquad (3)$$

where Q_{total} is the total charge passed during electrolysis with lignin, Q_{lignin} is the charge associated with direct lignin oxidation and Q_{blank} is the charge in the corresponding halide blank.

Based on this, the faradaic efficiency for lignin oxidation was calculated by:

$$FE_{lignin} = \frac{Q_{lignin}}{Q_{total}} \times 100\% \qquad (4)$$

Faradaic efficiency for oxygen evolution (FE_{O_2}) was derived from the amount of O_2 detected experimentally and converted to charge assuming a 4-electron process:

$$Q_{O_2} = 4Fn_{O_2} \qquad (5)$$

$$FE_{O_2} = \frac{Q_{O_2}}{Q_{total}} \times 100\% \qquad (6)$$

The residual fraction of the charge, not attributable to either lignin or oxygen oxidation, was assigned to halide oxidation:

$$FE_{halide} = 100\% - (FE_{lignin} + FE_{O_2}) \qquad (7)$$

In this context, two parallel oxidation pathways are therefore considered: (1) direct oxidation of lignin at the electrode quantified by FE_{lignin}, and (2) indirect oxidation *via* electro-generated iodine species approximated by FE_{halide}.

As shown in Table 3 for the iodide-containing systems, all three configurations (membrane-free, AEM, and CEM) exhibited high FE_{halide}, suggesting that the mediated pathway dominates the charge distribution in each case (further discussed in the next section). The consistently low FE_{O2} values highlight the advantage of BDD electrodes, which effectively suppress oxygen evolution even at high anodic potentials.[50]

However, when comparing FE values and total charge with the product yields in Table 1, no clear relationship was observed. For example, although the AEM and CEM systems exhibited similar total charges (338 *vs.* 330 C), the CEM yielded significantly more aromatic products. Likewise, the AEM system

showed the highest FE_{lignin} (27.5%) but lower yields than the CEM, while the membrane-free system had the highest FE_{halide} (93.3%) but the lowest product yields overall.

These findings imply that neither high direct oxidation (FE_{lignin}) nor high halide turnover (FE_{halide}) alone guarantees effective lignin depolymerization. Instead, the efficiency of mediated oxidation depends on whether oxidants generated through halide cycling are retained and react productively with lignin, rather than being lost to side reactions or physical crossover. The superior performance of the CEM system arises not from the absolute magnitude of FE_{halide} or FE_{lignin}, but from the selective confinement of redox-active iodine species, which improves the utilization efficiency of the mediated pathway and enhances net aromatic product yields. This interpretation is further supported by the presence of more deeply oxidized products, such as isovanillic acid and 2-furancarboxylic acid, which were detected only in CEM conditions. These findings highlight the critical role of membrane architecture in directing the electrochemical fate of lignin. The CEM configuration not only increased the total yield of aromatic products but also shifted the product profile toward deeper oxidative conversion.

3.4.2 Effect of halide mediators. The role of halide redox mediators in lignin electrooxidation was further investigated, as summarized in Table 4. In the chloride and bromide systems, the majority of the applied current was utilized for direct lignin oxidation, with FE_{lignin} of 88.6% and 74.1%, respectively. This indicates that lignin was oxidized predominantly *via* direct electron transfer at the BDD electrode surface. Halide oxidation contributed modestly (8.7% for Cl^-, 22.6% for Br^-), while oxygen evolution remained a minor side reaction (2.7–3.3%). These results are consistent with voltammetric observations (Section 3.2.2), where only modest changes in peak current were observed upon halide addition.

In contrast, the iodide system displayed a markedly different charge partitioning. Although it passed the highest total charge (330 C), only 65 C was associated with direct lignin oxidation (FE_{lignin} = 19.7%), while FE_{halide} = 79.3% dominated. This shift points to a mechanism governed by solution-phase mediated oxidation, where I^- is electrochemically converted to reactive species such as I_2, IO_3^-, and possibly IO_4^-, which oxidize lignin in bulk solution. This pathway is further supported by the suppression of electrode fouling (as the reaction takes place away from the electrode surface) and the higher aromatic product yields observed for the iodide system.

Efforts to directly quantify iodine intermediates under *operando* conditions proved analytically intractable in the present study. Ion-selective electrodes, while responsive under calibration, lacked sufficient resolution to detect the small

Table 3 Effect of membrane configuration on charge distribution and faradaic efficiency during electrochemical oxidation of alkaline lignin (20 g L^{-1}) at a BDD electrode in 1.0 M NaOH with 18 mM KI at 2.36 V *vs.* RHE, 25 °C, 4 h

Membrane	Q_{total} (C)	Q_{blank} (C)	Q_{lignin} (C)	FE_{O_2}	FE_{halide}	FE_{lignin}
None	231	218	13	1.1	93.3	5.6
Anion-exchange	338	245	93	1.4	71.1	27.5
Cation-exchange	330	265	65	1.0	79.3	19.7

Table 4 Effect of halide on charge distribution and faradaic efficiency during electrochemical oxidation of alkaline lignin (20 g L^{-1}) at a BDD electrode in 1.0 M NaOH with 18 mM halide at 2.36 V *vs.* RHE, 25 °C, 4 h

Halide	Q_{total} (C)	Q_{blank} (C)	Q_{lignin} (C)	FE$_{O_2}$ (%)	FE$_{halide}$ (%)	FE$_{lignin}$ (%)
Cl$^-$	176	20	156	2.7	8.7	88.6
Br$^-$	158	41	117	3.3	22.6	74.1
I$^-$	330	265	65	1.0	79.3	19.7

changes in free iodide concentration anticipated during electrolysis. The expected shifts (<5%) correspond to less than 1 mV, falling within the instrumental drift and rendering the measurements inconclusive. UV-vis spectroscopy was also unsuitable as the strong absorbance of lignin and its oxidation products in the 280–350 nm range overlapped with the diagnostic bands of triiodide and other iodine species, compromising spectral deconvolution. Attempts to use classical iodometric titrations (*e.g.* with thiosulfate) were unsuccessful due to uncontrolled redox reactions with phenolic moieties in the lignin matrix, which interfered with iodine chemistry and precluded selective quantification. More advanced analytical approaches such as *operando* spectroscopy may offer the ability to resolve individual iodine species and are recommended for future investigations.

Nevertheless, the convergence of multiple independent lines of evidence, namely, the exceptionally high faradaic efficiency for iodide oxidation, the sharply reduced direct electron transfer to lignin, the suppression of electrode fouling, and the enhanced monomer yields, collectively support the operation of a homogeneous, iodine-mediated oxidation pathway.[51,52] To the best of our knowledge, no alternative mechanism can reconcile these observations. Accordingly, while the identity and dynamics of the transient iodine intermediates remain unresolved, the mechanistic conclusion that I$^-$ acts as a redox shuttle in this system is robustly supported.

These results therefore suggest distinct oxidation regimes depending on halide identity. The chloride and bromide systems promote more direct electrochemical oxidation of lignin at the electrode surface, which can lead to significant electrode fouling and ultimately lower product yields. In contrast, the iodide system operates primarily through mediated oxidation pathways: iodide is electrochemically oxidized to I$_2$, which disproportionates in alkaline solution to form IO$_3^-$, and under extended oxidation, potentially IO$_4^-$.[36] These species are capable of oxidizing lignin in the solution phase without requiring direct contact with the electrode, thereby minimizing electrode fouling and resulting in high product yields.

It is worth noting that halide salts are often employed as supporting electrolytes under the assumption that they are electrochemically inert or used without a clear understanding of their mechanistic role.[53–55] However, in oxidative environments, especially under galvanostatic conditions in two-electrode systems, where potentials are not and cannot be precisely controlled, the redox activity of halides can significantly alter reaction pathways and outcomes. Our findings highlight the critical role of halide redox chemistry in dictating the course of

electrochemical lignin depolymerization to optimize reactivity and selectivity.

The environmental behavior of electrogenerated iodine species also warrants consideration. While reactive iodine species are inherently oxidizing and can be mildly corrosive at high concentrations, the alkaline and dilute conditions employed here (18 mM I$^-$) help stabilize these species. Under these conditions, I$_2$ is rapidly and efficiently converted to IO$_x^-$,[56] which are less volatile. In addition, the reactive iodine species generated are consumed through lignin oxidation, further limiting their accumulation. The use of a cation-exchange membrane confines iodide and its oxidation products within the anodic compartment, reducing the risk of uncontrolled release. Moreover, no iodinated aromatic compounds were detected in post-electrolysis solutions by GC-MS, supporting the safe and contained use of iodide as a redox mediator under the conditions studied.

This mediated system exhibited characteristics that may be favorable for future scale-up. Operating under mild aqueous conditions at ambient temperature and pressure, with modest energy requirements (*ca.* 0.08–0.11 kW h per kg lignin), the platform is compatible with continuous flow configurations. The use of BDD electrodes provides long-term chemical stability and resistance to fouling, especially in iodide-containing systems, while mediator regeneration and product extraction are straightforward. These attributes collectively highlight the feasibility of translating this process to larger-scale lignin valorization.

4 Conclusions

This work has identified key factors governing the electrochemical depolymerization of lignin, with an emphasis on the roles of electrode material, halide redox mediators, and membrane configurations. Cyclic voltammetry revealed that BDD enables efficient lignin electrooxidation with enhanced resistance to electrode fouling. The identity and concentration of halide mediators were found to exert significant effects on both voltammetric behavior and long-term electrolysis performance. Chloride and bromide systems facilitated direct electrode-driven oxidation, prone to surface passivation. In contrast, iodide enabled solution-phase mediated oxidation *via* electrogenerated iodine species, minimizing electrode fouling and yielding high aromatic product levels. These findings highlight a trade-off between electrochemical and chemical efficiency that depends on the choice of mediator. Membrane configuration also emerged as a critical design parameter. The use of a cation-exchange membrane significantly enhanced

both product yields and selectivity toward deeper oxidation products by confining reactive halogen species near the electrode interface, thereby prolonging their lifetimes and intensifying local oxidation. Collectively, these results establish a mechanistic framework for lignin electrooxidation and demonstrate that careful selection of halide mediator and membrane architecture enables tunable control over product distribution and depolymerization efficiency. This work offers valuable design principles for developing scalable, sustainable electrochemical platforms for lignin valorization, with broader applicability to other biopolymers.

Conflicts of interest

The authors declare no known competing financial interests or personal relationships that could have appeared to influence the work reported in this paper.

Data availability

The data used to support the findings of this study are included within the manuscript.

Acknowledgements

References

1 X. Du, H. Zhang, K. P. Sullivan, P. Gogoi and Y. Deng, Electrochemical lignin conversion, *ChemSusChem*, 2020, **13**(17), 4318–4343.

2 J. Olmstead and D. Gray, Fluorescence spectroscopy of cellulose, lignin and mechanical pulps: a review, *J. Pulp Pap. Sci.*, 1997, **23**(12), J571–J581.

3 P. C. R. Pinto, E. A. B. da Silva and A. r. E. d. Rodrigues, Insights into oxidative conversion of lignin to high-added-value phenolic aldehydes, *Ind. Eng. Chem. Res.*, 2011, **50**(2), 741–748.

4 A. Boarino and H.-A. Klok, Opportunities and Challenges for Lignin Valorization in Food Packaging, Antimicrobial, and Agricultural Applications, *Biomacromolecules*, 2023, **24**(3), 1065–1077.

5 M. Fortin, M. M. Beromi, A. Lai, P. C. Tarves, C. A. Mullen, A. A. Boateng and N. M. West, Structural analysis of pyrolytic lignins isolated from switchgrass fast-pyrolysis oil, *Energy Fuels*, 2015, **29**(12), 8017–8026.

6 Z. Li, J. Zhang, L. Qin and Y. Ge, Enhancing antioxidant performance of lignin by enzymatic treatment with laccase, *ACS Sustain. Chem. Eng.*, 2018, **6**(2), 2591–2595.

7 J. Luo and T. L. Liu, Electrochemical valorization of lignin: status, challenges, and prospects, *J. Bioresour. Bioprod.*, 2023, **8**(1), 1–14.

8 L. M. Lindenbeck, V. C. Barra, B. B. Beele, B. V. Rodrigues and A. Slabon, Revisiting the Electrocatalyst Role on Lignin Depolymerization, *Adv. Energy Sustain. Res.*, 2024, **5**(10), 2400130.

9 H. Oh, Y. Choi, C. Shin, T. V. T. Nguyen, Y. Han, H. Kim, Y. H. Kim, J.-W. Lee, J.-W. Jang and J. Ryu, Phosphomolybdic acid as a catalyst for oxidative valorization of biomass and its application as an alternative electron source, *ACS Catal.*, 2020, **10**(3), 2060–2068.

10 M. Breiner, M. Zirbes and S. R. Waldvogel, Comprehensive valorisation of technically relevant organosolv lignins via anodic oxidation, *Green Chem.*, 2021, **23**(17), 6449–6455.

11 J. Klein and S. R. Waldvogel, Selective Electrochemical Degradation of Lignosulfonate to Bio-Based Aldehydes, *ChemSusChem*, 2023, **16**(8), e202202300.

12 X. Xiao, S. Sun, Y. Qi, S. Hao, W. Zhang and X. Qiu, Selective electrocatalytic oxidation of C(OH)–C bond in lignin with Pt@CeO$_2$ toward the synthesis of benzoic acid, *Electrochim. Acta*, 2023, **470**, 143377.

13 P. Cai, H. Fan, S. Cao, J. Qi, S. Zhang and G. Li, Electrochemical conversion of corn stover lignin to biomass-based chemicals between Cu/NiMoCo cathode and Pb/PbO$_2$ anode in alkali solution, *Electrochim. Acta*, 2018, **264**, 128–139.

14 W. Liu, Y. Cui, X. Du, Z. Zhang, Z. Chao and Y. Deng, High efficiency hydrogen evolution from native biomass electrolysis, *Energy Environ. Sci.*, 2016, **9**(2), 467–472.

15 L. Mao, L. Zhang, N. Gao and A. Li, FeCl$_3$ and acetic acid co-catalyzed hydrolysis of corncob for improving furfural production and lignin removal from residue, *Bioresour. Technol.*, 2012, **123**, 324–331.

16 C. Smith, J. H. Utley, M. Petrescu and H. Viertler, Biomass electrochemistry: anodic oxidation of an organo-solv lignin in the presence of nitroaromatics, *J. Appl. Electrochem.*, 1989, **19**, 535–539.

17 P. Liewchirakorn and K. Ngamchuea, Benign electrolytic modifications of starch: effects on functional groups and physical properties, *RSC Adv.*, 2023, **13**(43), 30040–30051.

18 Y.-s. Wang, F. Yang, Z.-h. Liu, L. Yuan and G. Li, Electrocatalytic degradation of aspen lignin over Pb/PbO$_2$ electrode in alkali solution, *Catal. Commun.*, 2015, **67**, 49–53.

19 O. Y. Abdelaziz, I. Clemmensen, S. Meier, S. Bjelić, C. P. Hulteberg and A. Riisager, Oxidative depolymerization of Kraft Lignin to Aromatics over bimetallic V–Cu/ZrO$_2$ catalysts, *Top. Catal.*, 2023, **66**(17), 1369–1380.

20 O. Movil-Cabrera, A. Rodriguez-Silva, C. Arroyo-Torres and J. A. Staser, Electrochemical conversion of lignin to useful chemicals, *Biomass Bioenergy*, 2016, **88**, 89–96.

21 P. Xiu, X. Lu, D. Wang, J. Chen, C. Xu and X. Gu, Efficient depolymerization of alkaline lignin to phenolic monomers over non-precious bimetallic Ni–Fe/CeO$_2$-Al$_2$O$_3$ catalysts, *Biomass Convers. Biorefin.*, 2024, **14**(4), 4661–4675.

22 M. Sette, H. Lange and C. Crestini, Quantitative HSQC analyses of lignin: a practical comparison, *Comput. Struct. Biotechnol. J.*, 2013, **6**(7), e201303016.

23 R. C. Sun, Lignin source and structural characterization, *ChemSusChem*, 2020, **13**(17), 4385–4393.

24 M. Karlsson, J. Romson, T. Elder, Å. Emmer and M. Lawoko, Lignin structure and reactivity in the organosolv process studied by NMR spectroscopy, mass spectrometry, and density functional theory, *Biomacromolecules*, 2023, **24**(5), 2314–2326.

25 H. Kim and J. Ralph, Solution-state 2D NMR of ball-milled plant cell wall gels in DMSO-d_6/pyridine-d_5, *Org. Biomol. Chem.*, 2010, **8**(3), 576–591.

26 Z. Shen, Y. Liu, X. Wei, L. Zhang, L. Zeng, S. Wang and D. Min, Structural characteristics of eucalyptus lignin regulated through alkali cooking process, *Bioresources*, 2022, **17**(3), 4226.

27 E. A. Capanema, M. Y. Balakshin and J. F. Kadla, Quantitative characterization of a hardwood milled wood lignin by nuclear magnetic resonance spectroscopy, *J. Agric. Food Chem.*, 2005, **53**(25), 9639–9649.

28 C. Zhao, J. Huang, L. Yang, F. Yue and F. Lu, Revealing structural differences between alkaline and kraft lignins by HSQC NMR, *Ind. Eng. Chem. Res.*, 2019, **58**(14), 5707–5714.

29 L. B. Krivdin, NMR studies of lignin and lignin-derived products: recent advances and perspectives, *Russ. Chem. Rev.*, 2025, **94**(3), RCR5159.

30 W. Satianram, P. Sunon, B. Ngokpho, S. Nijpanich, N. Chanlek, T. Khotavivattana, C. Batchelor-McAuley and K. Ngamchuea, Electrochemical detection of melatonin at nano-sized highly boron-doped diamond electrode, *J. Electrochem. Soc.*, 2024, **171**(8), 087504.

31 K. Kaewket, C. Karuwan, S. Sonsupap, S. Maensiri and K. Ngamchuea, Anti-fouling effects of carbon nanofiber in electrochemical sensing of phenolic compounds, *J. Electrochem. Soc.*, 2021, **168**(6), 067501.

32 Y. Li, Y. Zhao, K. Chen, X. Liu, T. Yi and L.-F. Chen, Rational design of cross-linked N-doped C-Sn nanofibers as free-standing electrodes towards high-performance Li-ion battery anodes, *Acta Phys.-Chim. Sin.*, 2024, **40**(3), 2305007.

33 R. Oliveira, M. Mateus and D. Santos, On the oxidation of kraft black liquor for lignin recovery: a voltammetric study, *J. Electrochem. Soc.*, 2019, **166**(16), E547.

34 X. Liu, S. You, F. Ma and H. Zhou, Characterization of electrode fouling during electrochemical oxidation of phenolic pollutant, *Front. Environ. Sci. Eng.*, 2021, **15**, 1–10.

35 Y. Hou, K. J. Aoki, J. Chen and T. Nishiumi, Invariance of double layer capacitance to polarized potential in halide solutions, *Univers. J. Chem.*, 2013, **1**(4), 162–169.

36 M. Pourbaix, *Atlas of Electrochemical Equilibria in Aqueous Solutions*, NACE, 1966.

37 X. Liu, Y. Wang and H. Duan, Recent Progress in Electrocatalytic Conversion of Lignin: From Monomers, Dimers, to Raw Lignin, *Precis. Chem.*, 2024, **2**(9), 428–446.

38 D. Li, C. Lin, C. Batchelor-McAuley, L. Chen and R. G. Compton, Tafel analysis in practice, *J. Electroanal. Chem.*, 2018, **826**, 117–124.

39 N. McDonald, E. P. Achterberg, C. A. Carlson, M. Gledhill, S. Liu, J. R. Matheson-Barker, N. B. Nelson and R. J. Parsons, The role of heterotrophic bacteria and archaea in the transformation of lignin in the open ocean, *Front. Mar. Sci.*, 2019, **6**, 743.

40 R. Tolba, M. Tian, J. Wen, Z.-H. Jiang and A. Chen, Electrochemical oxidation of lignin at IrO_2-based oxide electrodes, *J. Electroanal. Chem.*, 2010, **649**(1–2), 9–15.

41 P. Atkins, *Shriver and Atkins' Inorganic Chemistry*, Oxford University Press, USA, 2010.

42 J. Ruwoldt, M. Tanase-Opedal and K. Syverud, Ultraviolet spectrophotometry of lignin revisited: exploring solvents with low harmfulness, lignin purity, hansen solubility parameter, and determination of phenolic hydroxyl groups, *ACS Omega*, 2022, **7**(50), 46371–46383.

43 D. Shao, J. Liang, X. Cui, H. Xu and W. Yan, Electrochemical oxidation of lignin by two typical electrodes: $Ti/SbSnO_2$ and Ti/PbO_2, *Chem. Eng. J.*, 2014, **244**, 288–295.

44 Y. Uruma, T. Yamada, T. Kojima, T. Zhang, C. Qu, M. Ishihara, T. Watanabe, K. Wakamatsu and H. Maekawa, Degradation of three β-O-4 lignin model compounds via organic electrolysis and elucidation of the degradation mechanisms, *RSC Adv.*, 2023, **13**(26), 17991–18000.

45 R. Ghahremani and J. A. Staser, Electrochemical oxidation of lignin for the production of value-added chemicals on Ni-Co bimetallic electrocatalysts, *Holzforschung*, 2018, **72**(11), 951–960.

46 N. Di Fidio, J. W. Timmermans, C. Antonetti, A. M. R. Galletti, R. J. Gosselink, R. J. Bisselink and T. M. Slaghek, Electro-oxidative depolymerisation of technical lignin in water using platinum, nickel oxide hydroxide and graphite electrodes, *New J. Chem.*, 2021, **45**(21), 9647–9657.

47 M. Liu, Y. Wen, J. Qi, S. Zhang and G. Li, Fine chemicals prepared by bamboo lignin degradation through electrocatalytic redox between Cu cathode and Pb/PbO_2 anode in alkali solution, *ChemistrySelect*, 2017, **2**(17), 4956–4962.

48 C. Lan, H. Fan, Y. Shang, D. Shen and G. Li, Electrochemically catalyzed conversion of cornstalk lignin to aromatic compounds: an integrated process of anodic oxidation of a Pb/PbO_2 electrode and hydrogenation of a nickel cathode in sodium hydroxide solution, *Sustain. Energy Fuels*, 2020, **4**(4), 1828–1836.

49 Y. Jia, Y. Wen, X. Han, J. Qi, Z. Liu, S. Zhang and G. Li, Electrocatalytic degradation of rice straw lignin in alkaline solution through oxidation on a $Ti/SnO_2–Sb_2O_3/\alpha\text{-}PbO_2/\beta\text{-}PbO_2$ anode and reduction on an iron or tin doped titanium cathode, *Catal. Sci. Technol.*, 2018, **8**(18), 4665–4677.

50 J. Sotelo-Gil, E. Cuevas-Yañez and B. A. Frontana-Uribe, Recent advances on boron doped diamond (BDD) electrode as cathode in organic and inorganic preparative electrotransformations, *Curr. Opin. Electrochem.*, 2022, **34**, 101004.

51 X. Liu, B. Tang, Y. Gao, X. Qi, F. Zhao, Z. Chen, Y. Zhu, H. Zheng and Y. Chu, Iodide-mediated electrosynthesis of 2, 6-dichlorobenzonitrile enhanced by acetate ions, *Electrochim. Acta*, 2025, **538**, 146922.

52 F. Lian, K. Xu and C. Zeng, Indirect electrosynthesis with halogen ions as mediators, *Chem. Rec.*, 2021, **21**(9), 2290–2305.

53 W. Deng, K. Xu, Z. Xiong, W. Chaiwat, X. Wang, S. Su, S. Hu, J. Qiu, Y. Wang and J. Xiang, Evolution of aromatic structures during the low-temperature electrochemical upgrading of bio-oil, *Energy Fuels*, 2019, **33**(11), 11292–11301.

54 M. Garedew, D. Young-Farhat, J. E. Jackson and C. M. Saffron, Electrocatalytic upgrading of phenolic compounds observed after lignin pyrolysis, *ACS Sustain. Chem. Eng.*, 2019, **7**(9), 8375–8386.

55 S. Dabral, H. Wotruba, J. G. Hernandez and C. Bolm, Mechanochemical oxidation and cleavage of lignin β-O-4 model compounds and lignin, *ACS Sustain. Chem. Eng.*, 2018, **6**(3), 3242–3254.

56 A. J. Bard, *Standard Potentials in Aqueous Solution*, CRC Press, 2017.